CHAPTER SIXTY EIGHT

COMBINED REFRACTION-DIFFRACTION OF NONLINEAR WAVES IN SHALLOW WATER

James T. Kirby,[1] Philip L.-F. Liu,[2] A.M's. ASCE

Sung B. Yoon[3] and Robert A. Dalrymple[4], M. ASCE

The parabolic approximation is developed to study the combined refraction/diffraction of weakly nonlinear shallow water waves. Two methods of approach are taken. In the first method Boussinesq equations are used to derive evolution equations for spectral wave components in a slowly varying two-dimensional domain. The second method modifies the equation of Kadomtsev & Petviashvili to include varying depth in two dimensions. Comparisons are made between present numerical results, experimental data and previous numerical calculations.

Introduction

In recent years, the recognition of the need for an improvement on the predictive capabilities of standard refraction methods (for example, Skovgaard, et al., 16) has led to the development of several techniques for computing wave fields modified by the combined effects of refraction and diffraction. Among these methods, the parabolic equation method (PEM) appears to be particularly attractive in the study of wave propagation in open coastal regions since its usefulness depends on a nearly unidirectional propagation of waves with little backscatter. The method was first developed for monochromatic linear waves by Radder (14) and Lozano & Liu (12) and has been extended to include effects such as frictional dissipation (3) and wave-current interaction (1,6,9). Recently, the formulation has been extended to the case of second-order monochromatic Stokes waves (8,11,19). Iterative methods have been developed in order to model the gradual development of reflected wave components, both for the linear (10) and Stokes wave (7) formulations.

Waves in shallow water near the coastline are rarely monochromatic, and are subject to fairly strong nonlinear interactions due to near-resonances as the phase speeds of individual spectral components approach coincidence. In addition, the smallness of the ratio of water

1. Assistant Professor, Marine Sciences Research Center, State Univ. of New York, Stony Brook, NY (presently, Coastal and Oceanographic Engineering Dept., Univ. of Florida, Gainesville, FL 32611).
2. Professor, School of Civil and Environmental Engineering, Cornell University, Ithaca, NY 14853.
3. Graduate Student, School of Civil and Envir. Engrg., Cornell Univ., Ithaca, NY 14853.
4. Professor, Dept. of Civil Engineering, University of Delaware, Newark, DE 19716.

depth to wavelength in such regions invalidates the assumptions underlying the Stokes theory and leads, instead, to a description of the wavefield based on the Korteweg-deVries or Boussinesq equations. For this reason, we have investigated methods for calculating the propagation and evolution of spectral wave components in an arbitrarily varying, two-dimensional domain, with the restrictions of shallow water and the parabolic approximation applied. The results of this study extend the PEM to the case of nonlinear waves in shallow water, and are applicable to the study of harmonic generation and spectral evolution as well as refraction-diffraction.

Two methods of approach are described. First, Boussinesq equations are used to derive evolution equations for spectral wave components in a slowly varying, two-dimensional domain. Secondly, we describe a similar modeling approach based on a version of the weakly two-dimensional Korteweg-deVries equation of Kadomtsev & Petviashvili (5) (hereafter referred to as the K-P equation). The present approach extends the K-P equation to include varying water depth in two dimensions. The resulting systems of coupled nonlinear partial differential equations for spectral wave components from two approaches are quite similar. These equations are written in finite difference form using the Crank-Nicolson method, yielding an initial-boundary value problem for the spatial evolution of each spectral mode.

The present model is used to examine the refraction of a cnoidal wave over a plane slope in a rectangular channel. Numerical solutions agree very well with previous analytical and numerical results. The formation of stem waves along the boundary and the development of a high-frequency modulation are observed and discussed. Comparisons are also made between the predictions of each model and the experimental data of Whalin (18) for his three second wave period case. The agreement between experimental data and numerical results is reasonable but not excellent. Both models predict much higher first harmonic amplitudes along the centerline of the tank. The prediction of the second and third harmonic amplitudes is seen to be better.

Nonlinear Shallow-Water Wave Equations and Parabolic Approximation

The Boussinesq equations, which include nonlinearity and dispersion to the leading order, are used as a basis of the first approach. Using ω as the characteristic frequency, a_o as the characteristic wave amplitude and h_o as the characteristic water depth, we introduce the following dimensionless variables:

$$t = \omega t' \quad , \quad (x,y) = \frac{\omega}{\sqrt{gh_o}} (x',y') \quad , \quad z = z'/h_o$$

$$h = h'/h_o \quad , \quad \vec{u} = \vec{u}'/[\frac{a_o}{h_o} \sqrt{gh_o}] \quad , \quad \zeta = \zeta'/a_o \tag{1}$$

where ζ is the free surface displacement and $\vec{u}$ represents the depth-averaged horizontal velocity vector. The quantities with prime denote dimensional quantities. If the scale of water depth is small in comparison with the horizontal length scale and the wave amplitude is small compared with the water depth, i.e.,

$$\mu^2 = \omega^2 h_o/g \ll 1 \tag{2}$$

$$\varepsilon = a_o/h_o \ll 1 \tag{3}$$

the Boussinesq equations take the following dimensionless forms:

$$\frac{\partial\zeta}{\partial t} + \nabla\cdot[(h+\varepsilon\zeta)\vec{u}\,] = O(\varepsilon^2,\ \varepsilon\mu^2,\ \mu^4) \tag{4}$$

$$\frac{\partial\vec{u}}{\partial t} + \varepsilon\vec{u}\cdot\nabla\vec{u} + \nabla\zeta = \mu^2\ \{\frac{1}{2}\,h\,\frac{\partial}{\partial t}\,\nabla[\nabla\cdot(h\vec{u})] - \frac{1}{6}\,h^2\,\frac{\partial}{\partial t}\,\nabla(\nabla\cdot\vec{u})\} + O(\varepsilon^2,\ \varepsilon\mu^2,\ \mu^4) \tag{5}$$

where two small parameters, ε and μ^2, are assumed to be of the same order of magnitude. In the present study we also assume that the variation of water depth is small in a characteristic wavelength, i.e., $O(|\nabla h|) \leq O(\mu^2)$.

We shall study the propagation of a shallow water wave train which is periodic in time with the fundamental frequency ω. The solutions can be expressed as a Fourier series

$$\zeta(x,y,t) = \frac{1}{2}\sum_n \zeta_n(x,y)e^{-int}\quad,\quad n=0,\ \pm1,\ \pm2,\ \ldots \tag{6}$$

$$\vec{u}(x,y,t) = \frac{1}{2}\sum_n \vec{u}_n(x,y)e^{-int}\quad,\quad n=0,\ \pm1,\ \pm2,\ \ldots \tag{7}$$

where $(\zeta_{-n},\ \vec{u}_{-n})$ are the complex conjugates of $(\zeta_n,\ \vec{u}_n)$. Substituting eqs. (6) and (7) into eqs. (4) and (5) and collecting the coefficients of different Fourier components yields the set of equations

$$-in\ \zeta_n + \nabla\cdot(h\ \vec{u}_n) + \frac{\varepsilon}{2}\sum_s \nabla\cdot(\zeta_s\ \vec{u}_{n-s}) = O(\varepsilon^2,\varepsilon\mu^2,\mu^4) \tag{8}$$

$$-in\ \vec{u}_n + (1 - \frac{\mu^2 n^2}{3}\,h)\nabla\zeta_n + \frac{\varepsilon}{4}\sum_s\ (\vec{u}_s\cdot\vec{u}_{n-s}) = O(\varepsilon^2,\varepsilon\mu^2,\mu^4) \tag{9}$$

where $s = 0,\ \pm1,\ \pm2,\ \ldots$. From these two equations we can find the following lowest order relationships:

$$\vec{u}_n = -\frac{i}{n}\,\nabla\zeta_n[1 + O(\varepsilon,\mu^2)] \tag{10}$$

$$\nabla\cdot\vec{u}_n = in\ \zeta_n/h[1 + O(\varepsilon,\mu^2)] \tag{11}$$

for $n \neq 0$, and

$$\vec{u}_o = -\frac{\varepsilon}{2h}\sum_s \zeta_s\ \vec{u}_{-s} + O(\varepsilon^2,\mu^4,\varepsilon\mu^2) \tag{12}$$

$$\zeta_o = -\frac{\varepsilon}{4}\sum_s \vec{u}_s \cdot \vec{u}_{-s} + O(\varepsilon^2,\mu^4,\varepsilon\mu^2) \tag{13}$$

For the case where water depth is a constant, h = 1, eqs. (8) and (9) reduce to those derived by Rogers & Mei (15).

Using eqs. (10) and (11) in eqs. (8) and (9) and eliminating $\vec{u}_n$ gives

$$\nabla\cdot[(h - \frac{\mu^2 n^2 h^2}{3})\nabla\zeta_n] + n^2\zeta_n = \frac{\varepsilon}{2h}\{\sum_s (n^2-s^2)\zeta_s\zeta_{n-s} - h\sum_{s\neq n}(\frac{n+s}{n-s})\nabla\zeta_s\cdot\nabla\zeta_{n-s} - 2h^2\sum_{\substack{s\neq 0\\ s\neq n}}\frac{1}{s(n-s)}(\frac{\partial^2\zeta_s}{\partial x^2}\frac{\partial^2\zeta_{n-s}}{\partial y^2} - \frac{\partial^2\zeta_s}{\partial x\partial y}\frac{\partial^2\zeta_{n-s}}{\partial x\partial y})\} + O(\varepsilon^2,\varepsilon\mu^2,\mu^4) \tag{14}$$

which constitutes a system of nonlinear equations for ζ_n (n = 1,2, 3,...). Since eq. (14) is a differential equation of the elliptic type, appropriate boundary conditions must be assigned along the boundaries. Once ζ_n (n = 1,2,...) are found, eq. (10) can be used to calculate the velocity vector $\vec{u}_n$. The mean free surface set-up or set-down, ζ_o, is obtained from eq. (13).

We now consider the cases where the dominant wave propagation direction is known and is in the x-direction. The free surface displacement for the n-th harmonic can be written as

$$\zeta_n = \psi_n(x,y)e^{inx} \tag{15}$$

where $\psi_n(x,y)$ denotes the amplitude function which takes both refraction and diffraction effects into account. Substitution of eq. (15) into eq. (14) yields

$$G_n(\frac{\partial^2\psi_n}{\partial x^2} + \frac{\partial^2\psi_n}{\partial y^2}) + (2in\,G_n + \frac{\partial G_n}{\partial x})\frac{\partial\psi_n}{\partial x} + \frac{\partial G_n}{\partial y}\frac{\partial\psi_n}{\partial y}$$

$$+ (in\frac{\partial G_n}{\partial x} - n^2 G_n + n^2)\psi_n = \frac{\varepsilon}{2h}\{\sum_s [h\,s(n+s) + (n^2-s^2)]\,\psi_s\psi_{n-s}$$

$$- h\sum_{s\neq n}(\frac{n+s}{n-s})[\nabla\psi_s\cdot\nabla\psi_{n-s} + i\,s\psi_s\frac{\partial\psi_{n-s}}{\partial x} + i(n-s)\,\psi_{n-s}\frac{\partial\psi_s}{\partial x}]$$

$$- 2h^2\sum_{\substack{s\neq 0\\ s\neq n}}\frac{1}{s(n-s)}[\frac{\partial^2\psi_s}{\partial x^2}\frac{\partial^2\psi_{n-s}}{\partial y^2} - \frac{\partial^2\psi_s}{\partial x\partial y}\frac{\partial^2\psi_{n-s}}{\partial x\partial y}$$

$$- s^2\psi_s\frac{\partial^2\psi_{n-s}}{\partial y^2} + s(n-s)\frac{\partial\psi_s}{\partial y}\frac{\partial\psi_{n-s}}{\partial y} + i(2s\frac{\partial\psi_s}{\partial x}\frac{\partial^2\psi_{n-s}}{\partial y^2}$$

$$- s\frac{\partial\psi_s}{\partial y}\frac{\partial^2\psi_{n-s}}{\partial x\partial y} - (n-s)\frac{\partial^2\psi_s}{\partial x\partial y}\frac{\partial\psi_{n-s}}{\partial y})] + O(\mu^4,\varepsilon\mu^2,\varepsilon^2) \tag{16}$$

where

$$G_n = h - \frac{\mu^2 n^2 h^2}{3} \tag{17}$$

In principle, eq. (16) can be solved as a system of boundary value problems for ψ_n.

The amplitude function ψ_n is primarily a function of the water depth due to wave shoaling. Therefore, ψ_n varies slowly in the direction of wave propagation at the same rate as that of h in the x-direction. Thus

$$\frac{\partial \psi_n}{\partial x} \sim \frac{\partial h}{\partial x} \sim O(\varepsilon, \mu^2) \tag{18}$$

$$\frac{\partial^2 \psi_n}{\partial x^2} \sim O(\varepsilon^2, \mu^4, \varepsilon\mu^2) \tag{19}$$

The diffraction effects are considered important. Hence,

$$\frac{\partial \psi_n}{\partial y} \sim O(1) \tag{20}$$

Using eqs. (18-20), we can simplify eq. (16) significantly to get

$$2in \frac{\partial \psi_n}{\partial x} + \frac{\partial^2 \psi_n}{\partial y^2} + \frac{1}{G_n} \frac{\partial G_n}{\partial y} \frac{\partial \psi_n}{\partial y} + [\frac{in}{G_n} \frac{\partial G_n}{\partial x} - n^2 (1 - \frac{1}{G_n})] \psi_n$$

$$= \frac{\varepsilon}{2hG_n} \{\sum_s [h\, s(n+s) + n^2 - s^2] \psi_s \psi_{n-s} - h \sum_{s \neq n} (\frac{n+s}{n-s}) \frac{\partial \psi_s}{\partial y} \frac{\partial \psi_{n-s}}{\partial y}$$

$$+ 2h^2 \sum_{s \neq n} \frac{1}{n-s} [s\, \psi_s \frac{\partial^2 \psi_{n-s}}{\partial y^2} - (n-s) \frac{\partial \psi_s}{\partial y} \frac{\partial \psi_{n-s}}{\partial y}]\} \tag{21}$$

Significantly, we have converted a set of elliptic equations (16) into a set of parabolic equations, (21), which may be solved with efficient numerical techniques. For later use, we can rewrite eq. (21) in a dimensional form

$$2in\, k_o \frac{\partial \psi_n}{\partial x} + \frac{1}{\bar{G}_n} \frac{\partial}{\partial y} (\bar{G}_n \frac{\partial \psi_n}{\partial y}) + \frac{1}{\bar{G}_n} (in\, k_o \frac{\partial \bar{G}_n}{\partial x} - n^2 k_o^2 \bar{G}_n + \frac{n^2 \omega^2}{g}) \psi_n$$

$$= \frac{1}{\bar{G}_n} \{\frac{1}{2} \sum_s [k_o^2\, s(n+s) + \frac{\omega^2}{gh} (n^2 - s^2)] \psi_s \psi_{n-s} - \frac{1}{2} \sum_{s \neq n} (\frac{n+s}{n-s})$$

$$\frac{\partial \psi_s}{\partial y} \frac{\partial \psi_{n-s}}{\partial y} + \sum_{s \neq n} \frac{g\, k_o^2\, h}{\omega^2 (n-s)} [s \psi_s \frac{\partial^2 \psi_{n-s}}{\partial y^2} - (n-s) \frac{\partial \psi_s}{\partial y} \frac{\partial \psi_{n-s}}{\partial y}]\} \tag{22}$$

where

$$\bar{G}_n = h(1 - \frac{n^2 \omega^2 h}{3g}) \tag{23}$$

is the dimensional form of eq. (17) and

$$k_o = \frac{\omega}{\sqrt{g\,h_o}} \tag{24}$$

is the wave number associated with a reference constant water depth h_o.

The Crank-Nicolson method is used to rewrite the governing differential equations, (21), in a finite difference form. The forward difference scheme is employed in the x-direction, which is a time-like variable, and a centered difference scheme is used in the y-direction. Details are similar to those given by Liu and Tsay (11) and are omitted here.

An Alternate Approach Based on the K-P Equation

The application of the parabolic approximation to the more general Boussinesq equations involves an implied restriction to the case of waves with a unidirectional propagation direction and small transverse modulation. In this connection, it is of some interest to examine model equations with time dependence incorporated which embody the same basic assumption. For the case of shallow water and constant depth, an equation of this form has been developed by Kadomtsev & Petviashvili (5). The K-P equation may be written (following Bryant, 2) as

$$\frac{\partial}{\partial x}\left(\frac{\partial \zeta}{\partial t} + \frac{\partial \zeta}{\partial x} + \frac{3\varepsilon}{2}\zeta\frac{\partial \zeta}{\partial x} + \frac{\mu^2}{6}\frac{\partial^3 \zeta}{\partial x^3}\right) + \frac{1}{2}\frac{\partial^2 \zeta}{\partial y^2} = O(\varepsilon^2, \varepsilon\mu^2, \mu^4) \tag{25}$$

The connection to the parabolic approximation may be seen by considering only O(1) terms and making the substitution

$$\zeta = \psi(x,y)e^{i(x-t)} \tag{26}$$

yielding (after assuming $O(\partial^2\psi/\partial x^2) << O(\partial\psi/\partial x)$)

$$2i\frac{\partial \psi}{\partial x} + \frac{\partial^2 \psi}{\partial y^2} = 0 \tag{27}$$

which is the parabolic approximation of the Helmholtz equation (Yue & Mei, 19). The K-P equation, which extends the Korteweg-deVries equation to include weak transverse modulations, thus contains the same degree of information as the parabolic approximation.

Based on this correspondence, we may construct a version of the K-P equation for variable depth. Retaining dimensional quantities, the resulting model equation may be written as

$$\frac{\partial}{\partial x'}\left(\frac{1}{C'}\frac{\partial \zeta'}{\partial t'} + \frac{\partial \zeta'}{\partial x'} + \frac{1}{4h'}\frac{\partial h'}{\partial x'}\zeta' + \frac{3}{2h'}\zeta'\frac{\partial \zeta'}{\partial x'} + \frac{(h')^2}{6}\frac{\partial^3 \zeta'}{\partial x'^3}\right.$$

$$\left. + \frac{1}{2h'}\frac{\partial}{\partial y'}\left(h'\frac{\partial \zeta'}{\partial y'}\right)\right) = 0 \tag{28}$$

where $C' = \sqrt{gh'}$. Neglecting y derivatives, the equation reduces to the form given by Johnson (4) after non-dimensionalization. Retaining only lowest order terms, making the substitution (where we drop primes for convenience),

$$\zeta = \overline{\psi}(x,y)e^{i(\int k dx - \omega t)} \tag{29}$$

$$\omega = C'k \tag{30}$$

and referencing the phase function to a constant value k_o (following Kirby & Dalrymple, 8) leads to the parabolic approximation

$$2ikh \frac{\partial\psi}{\partial x} + 2\, kh(k-k_o)\psi + i\, \frac{\partial(kh)}{\partial x}\psi + \frac{\partial}{\partial y}\,(h\,\frac{\partial\psi}{\partial y}) = 0 \tag{31}$$

which is simply the shallow water limit of the linear approximation

$$2ik\, CC_g \frac{\partial\psi}{\partial x} + 2k\, CC_g(k-k_o)\psi + i\,\frac{\partial}{\partial x}\,(k\, CC_g)\psi + \frac{\partial}{\partial y}\,(CC_g\,\frac{\partial\psi}{\partial y})=0 \tag{32}$$

obtained by Kirby & Dalrymple (8). In eq. (32) $C_g = \partial\omega/\partial k$ is the group velocity.

Before substituting a series expansion for ζ, it is advantageous to alter the dispersive term $\partial^3\zeta/\partial x^3$ by the following substitution

$$\frac{\partial^2\zeta}{\partial t^2} - g\,\frac{\partial}{\partial x}\,(h\,\frac{\partial\zeta}{\partial x}) = O(\varepsilon,\mu^2) \tag{33}$$

yielding the modified equation

$$\frac{\partial}{\partial x}\,\{\frac{1}{C}\,\frac{\partial\zeta}{\partial t} + \frac{\partial\zeta}{\partial x} + \frac{1}{4h}\,\frac{\partial h}{\partial x}\,\zeta + \frac{3}{\partial h}\,\zeta\,\frac{\partial\zeta}{\partial x}\} + \frac{h}{6C^2}\,\frac{\partial^3}{\partial t^2\partial x}\,(h\,\frac{\partial\zeta}{\partial x})$$
$$+ \frac{1}{2h}\,\frac{\partial}{\partial y}\,(h\,\frac{\partial\zeta}{\partial y}) = 0 \tag{34}$$

which has approximately the same dispersion relation as the set of equations (4) and (5). The parabolic approximation is obtained in similar fashion to the procedure of the previous section; we proceed using the slightly revised form

$$\zeta = \frac{1}{2}\sum_{n=-\infty}^{\infty} \overline{\psi}_n(x,y)e^{in(\int k dx - \omega t)} \tag{35}$$

to manipulate eq. (34) initially, after which a shift to a reference depth is employed (as in eq. 31) to obtain

$$2in\, k_o\,\frac{\partial\psi_n}{\partial x} + \frac{k_o}{k\,\overline{G}_n}\,\frac{\partial}{\partial y}\,(h\,\frac{\partial\psi_n}{\partial y}) + \frac{1}{\overline{G}_n}\,[\frac{in\,k_o}{2}\,\frac{\partial\overline{G}_n}{\partial x} - 2n^2k_o(k_o-k)\overline{G}_n$$

$$+ \frac{n^4}{3}\,(\frac{k_o}{k})\,\frac{\omega^4 h}{g}]\psi_n = \frac{3n^2k\,k_o}{4\overline{G}_n}\,[\sum_{s=1}^{n-1}\psi_s\psi_{n-s} + 2\sum_{s=1}^{N-n}\psi_{-s}\psi_{n+s}];$$

$$1 \le n \le N \tag{36}$$

where

$$\zeta = \frac{1}{2} \sum_{n=-\infty}^{\infty} \psi_n(x,y)e^{in(k_o x-\omega t)} \tag{37}$$

and where $\bar{G}_n$ and k_o are defined previously. The difference in the coefficients of ψ_n in eqs. (22) and (36) is accounted for by the fact that the substitution (37) is used throughout the entire process to obtain eq. (22) rather than the intermediate form, eq. (35).

Comparing eq. (36) to the corresponding equation (22), derived from the Boussinesq equation, we observe that the basic characteristics of these equations are the same. We remark, however, that in the approach using the K-P equation the nonlinearity is localized due to the original form of the equation (no y-derivatives in nonlinear term), and that the retention of only the lowest-order depth dependence in the y-derivative term implies a possible error in energy flux conservation and refraction for waves shoaling over a general two-dimensional topography. This latter effect could be alleviated by making the substitution $\partial(\bar{G}_n \partial\psi_n/\partial y)/\partial y$ for the given term in eq. (36). However, numerical experiments for the case of Whalin's experiment (18) have shown that this effect is not important to the present study.

Refraction of Waves over a Plane Slope

Both of the models derived here are strictly applicable to the case of waves propagating over topography which is very slowly varying in comparison to the fundamental wavelength. Experimental data which satisfies this criterion is lacking due to the large wave basin needed. Therefore, we first compare the present model's results to a case for which computational results are available. Such a case has been provided by Skovgaard & Peterson (17), who used the properties of a very slowly-varying train of cnoidal waves to develop a theory for the refraction and shoaling of obliquely incident waves on a plane beach. This situation has also been studied recently by Madsen & Warren (13), who obtained a numerical solution for the case of waves propagating in a rectangular channel containing a plane slope oriented at an angle of 26.6° to the channel side walls. Madsen & Warren used a time-dependent, finite difference solution of a set of conservation laws equivalent to eqs. (4) and (5) to obtain their numerical results. Here, we use the parameters chosen by Madsen & Warren and study the same channel configuration; however, we neglect the lateral boundary damping employed by Madsen & Warren in order to study the details of the reflection process at the vertical, impermeable side walls. The computational domain is given by $0 \leq x \leq 2154.5$, $0 \leq y \leq 1534.5$, with waves normally incident at $x = 0$. Slope-oriented coordinates are given by

$$\begin{aligned} x' &= (x - 420) \cos (26.6°) - (y - 775) \sin (26.6°) \\ y' &= (x - 420) \sin (26.6°) + (y - 775) \cos (26.6°) \end{aligned} \tag{38}$$

with water depth given by

$$h(x',y') = \begin{cases} 21 \text{ m} & ; \quad x' < 0 \\ (21 - 0.013\ x')\text{m} & ; \quad 0 \leq x' \leq 1076.9 \text{ m} \\ 7 \text{ m} & ; \quad x' > 1076.9 \text{ m} \end{cases} \tag{39}$$

Wave parameters for the problem are given by

T = 17.3 s = wave period
H = 1.74 m = wave height at 21 m depth

which gives a deepwater wavelength L_o = 467.1 m and an Ursell number $U_r = (H/2h)/(kh)^2 = 0.13$ in the deepwater portion of the channel. Initial conditions for the calculation are thus specified according to a third order Stokes wave at $x = 0$. A total of $N = 6$ components are retained, and the computational domain is divided into a rectangular grid with $\Delta x = \Delta y = 15.5$ m.

A plot of the model topography is given in Figure 1 along with a snapshot of the instantaneous water surface elevation, with contour increments of 1 m for bottom topography and 0.4 m for surface elevation. As the wave shoals, refraction effects are apparent in the center of the channel, and the wave develops from nearly sinusoidal form to shallow water profiles with narrow crests and broad troughs. The formation of a "Mach Stem" is apparent on the right boundary, where refraction turns the incident wave towards the wall, inducing a grazing-incidence reflection as in the study of Yue & Mei (19). Also apparent is the development of a high-frequency modulation, possibly consisting of an un-phaselocked higher mode, which evolves in the shallower portion of the tank. This short wave component causes a significant modulation of waveheight $H(x,y)$ in the shallow (h = 7 m) portion of the domain.

A plot of normalized waveheight H/h versus normalized water depth h/L_o for y = 750 m is given in Figure 2 in comparison to the refraction model of Skovgaard & Peterson (17) and the time-dependent numerical results of Madsen and Warren (13). The evolution of H/h is seen to be quite smooth up to the shallower depths, with the plotted points (corresponding to every fifth computational point) agreeing quite well with the refraction theory. In the shallow portion of the tank, the short wave modulation causes a significant variation in local wave height about the theoretical value. Wave height H was obtained by stepping the individual components through time to construct $\zeta'(x,y,t)$ and then determining $H(x,y)$ according to $\zeta'_{max} - \zeta'_{min}$.

Refracted angles of incidence between the wave and slope also agreed quite well with the refraction model and are not shown.

Plots of the water surface profile along the line y = 750 and through the "Mach Stem" region y = 0 are shown in Figures 3a and b, respectively. In both cases, results show the presence of separate peaks in the wave troughs; this was also noted in the results of Madsen & Warren and was attributed to truncation errors. The rapid evolution of a nearly uniform wave train is evident in the Mach-stem region in Figure 1. We remark that, due to the narrowness of the wave

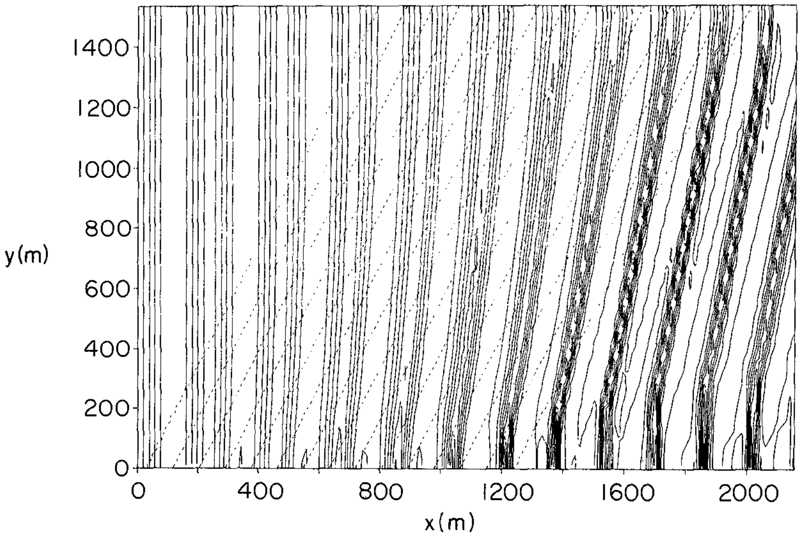

Figure 1. Bottom topography and contours of instantaneous surface elevation at t = 0; - - - - bottom contours in increments of 1 m, 7 m < h < 21 m, ——— contours of free surface elevation in increments of 0.4 m.

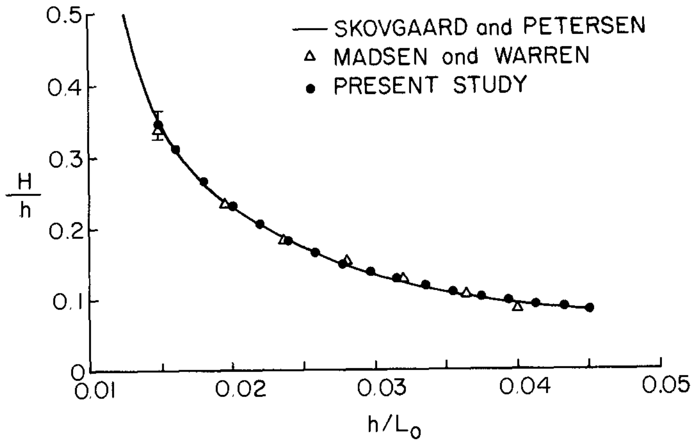

Figure 2. Normalized waveheight H/h as a function of h/L_o; error bar Φ at h/L_o = 0.015 indicates range of H values in shallow part of tank due to short wave modulation.

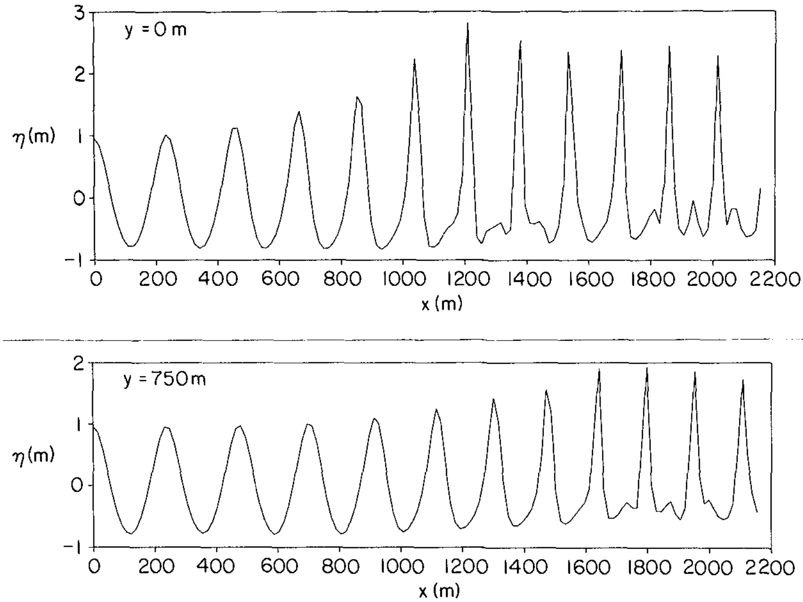

Figure 3. Free surface profiles for cnoidal wave refraction: (a) along y = 0 m, sidewall and through Mach stem region, and (b) along y = 750 m, near the centerline of channel.

crests, displacement of these crests away from actual computational grid points may contribute significantly to the modulation of crest elevations ζ'_{max} which is apparent in the plotted results.

We remark that increasing the number of modes without a further reduction of grid size did not significantly alter the results of this example. Tests with smaller grid size have not yet been conducted.

Wave Focusing By a Topographical Lens

Whalin (18) conducted a series of laboratory experiments concerning wave convergence over a bottom topography that acts as a focusing lens. The wave tank used in the experiments has the horizontal dimensions 25.603 m x 6.096 m. In the middle portion of the wave tank, 7.62 m < x < 15.24 m, eleven semicircular steps were evenly spaced and led to the shallower portion of the channel (Figure 4). The equations approximating the topography are given as follows:

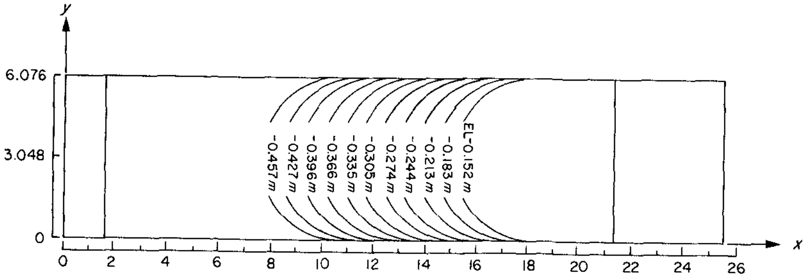

Figure 4. Topographical lens in Whalin's (18) wave tank experiments.

$$h(x,y) = \begin{cases} 0.4572 \text{ m} & (0 \le x < 10.67 - G(y)) \\ 0.4572 + \frac{1}{25}(10.67-G-x) \text{ m} & (10.67-G \le x \le 18.29 - G) \\ 0.1524 \text{ m} & (18.29 - G \le x \le 21.34) \end{cases} \quad (40)$$

where

$$G(y) = [y(6.096 - y)]^{1/2}\text{m} \qquad (0 \le y \le 6.096 \text{ m}) \qquad (41)$$

The bottom topography is symmetric with respect to the centerline of the wave tank, $y = 3.048$ m.

A wavemaker was installed at the deeper portion of the channel where the water depth h_o is 0.4572 m. Three sets of experiments were conducted by generating waves with periods T = 1, 2, and 3 secs., respectively. Different wave amplitudes were generated for each wave period. For the cases of T = 1 and 2 secs., a second order Stokes wave theory (11) has been shown to describe the combined refraction-diffraction mechanisms adequately. The focusing of water waves by refraction led to a focal region, in which energy was transferred to the second harmonic. For the experimental set with T = 3s the Ursell parameter, $U_r = (a/h)/(kh)^2$, is generally greater than unity in the shallower water region, which indicates that the Stokes wave theory is no longer valid and the present shallow water wave theory should be used. In Table 1, we summarize the experimental data and the corresponding small parameters ε and μ^2. The water depth in the shallower region, h_1 = 0.1524 m, has been used as the water depth scale.

Wave Period T(s)	Incident Wave Amplitude a_o(cm)			$\varepsilon = a_o/h_1$			$\mu^2 = \omega^2 h_1/g$
3.0	0.68	0.98	1.46	0.0446	0.0643	0.0958	0.0682

Table 1. Experimental and Numerical Parameters

According to Whalin's report, the second and the third harmonic waves grow rapidly in the focal zone. In fact, the ampli-tude of the higher harmonics becomes larger than that of the first harmonic (see Figures 5 and 6). To study this problem, we obtain numerical solutions by using both approaches described above. In numerical computations for each model, five harmonics ($N = 5$) are considered.

Owing to the symmetry of the problem with respect to the centerline of the wave tank, only one half of the wave tank is discretized. The computational domain starts from the wavemaker, $x = 0$, and ends at $x = 22$ m. The no-flux boundary conditions are used along the side wall and the centerline of the wave tank, i.e.

$$\frac{\partial \psi_n}{\partial y} = 0 \qquad \text{along } y = 0 \text{ and } 3.048 \text{ m} \tag{42}$$

for all n. The wave amplitude for the first harmonic waves at the wavemaker ($x = 0$) is prescribed with the values shown in Table 1. The initial conditions for higher harmonic waves are zero.

In numerical computations different grid sizes are tested for the convergence of the numerical scheme. Numerical solutions presented here are obtained by using $\Delta x = 0.25$ m and $\Delta y = 0.3048$ m, although no noticeable differences are observed when the grid sizes are doubled.

In Figure 5a, numerical results based on the Boussinesq equation approach for the case with $\varepsilon \approx 0.0446$, $\mu^2 = 0.0682$ and $a_o = 0.0068$ m are presented with experimental data. Wave amplitudes along the centerline of the wave tank are plotted. Since it is assumed that only the first harmonic waves are generated at the wavemaker, the wave energy in the higher harmonic components are sufficiently small over the constant depth region ($0 < x < 8$ m). However, as waves start to refract over the topography and focus along the centerline of the tank, a significant amount of energy is transferred into higher harmonic components. The agreement between laboratory data and numerical solutions is reasonable. The numerical model overestimates the first harmonic amplitudes. The second and third harmonic wave amplitudes are in good agreement with reported data. (Several experiments with higher values of N indicated only minor changes for modes 1-3.) Results for the cases $a_o = 0.0098$ m ($\varepsilon = 0.0643$, μ^2, $= 0.0682$) and $a_o = 0.0146$ m ($\varepsilon = 0.0958$, $\mu^2 = 0.0682$) are shown in Figures 5b and 5c, respectively. Again, the model uniformly overpredicts first harmonic amplitude along the channel centerline, although the amplitude of the second harmonic is well-predicted in both cases. The third harmonic amplitude is also well-predicted in Figure 5b. The high-amplitude case of Figure 5c indicates a tendency for the numerical result to undergo the start of a recurrence behavior before the experimental maximum of ζ_3 is obtained.

Numerical results for the three cases presented above were also obtained using the K-P model with $N = 5$. Here, h_o and k_o are taken to correspond to the shallow portion of the tank. To compare these

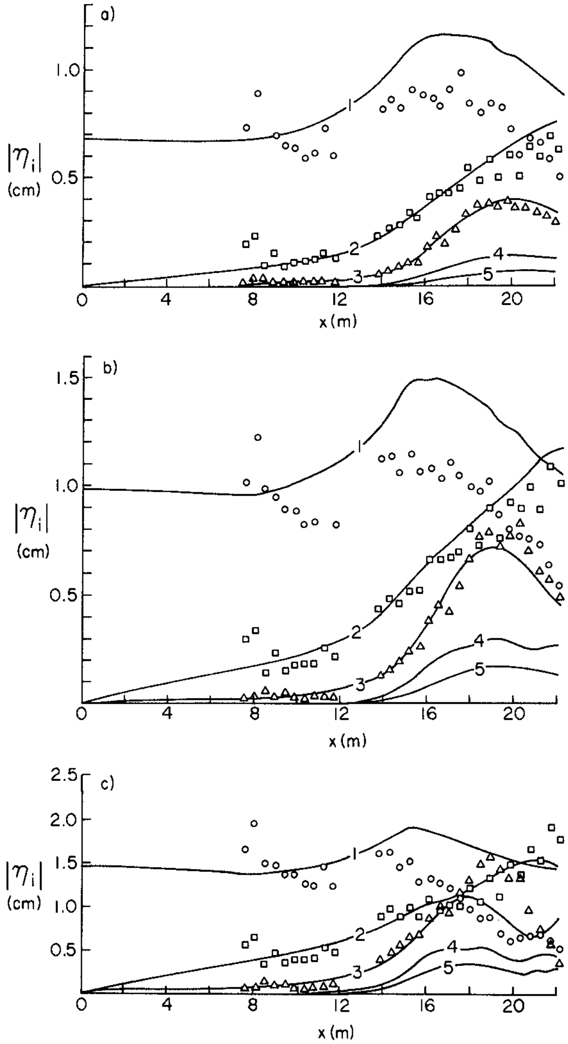

Figure 5. Harmonic amplitudes along centerline of Whalin's channel. a) a_o = 0.68 cm, b) a_o = 0.98 cm, c) a_o = 1.46 cm. Results using equation (21).

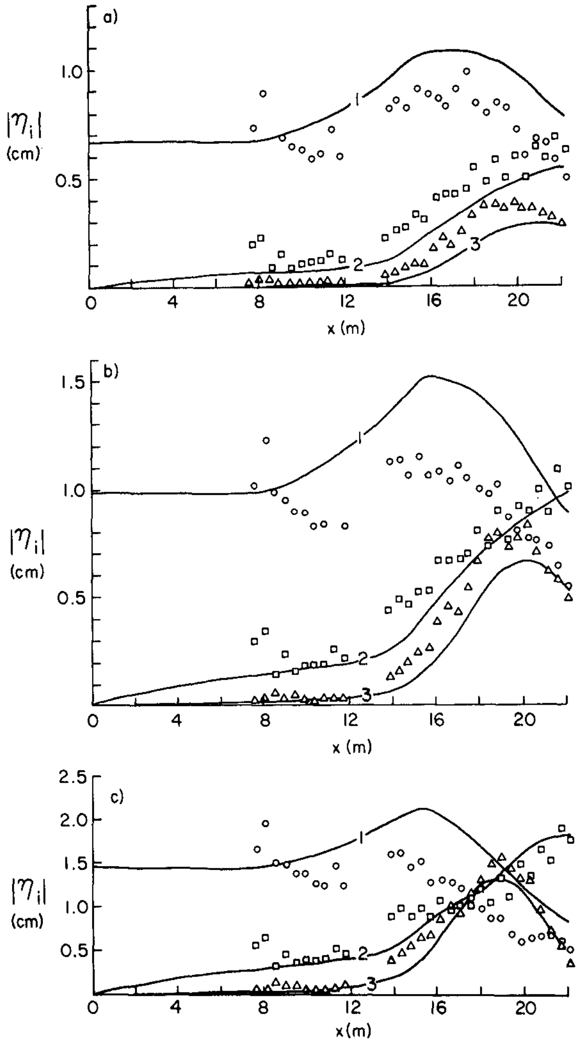

Figure 6. As in Figure 5. Results using equation (36).

two models, numerical solutions for the first three harmonics are shown in Figure 6a-c. For the low amplitude case $a_o = 0.68$ cm (Figure 6a), the results from the K-P model show an underprediction of second and third harmonic amplitudes, indicating the possible effect of the lowest-order y derivative term given in eq. (36). For the higher amplitude case (Figure 6b and c), nonlinearity becomes relatively more important and results of the two models are in closer agreement, with the exception that harmonic amplitudes grow somewhat more slowly in the K-P model. Both models are seen to be capable of predicting the essential features of harmonic generation in the focusing of a nonlinear wave. We remark that results of each model are sensitive to the choice of initial conditions, so that more detailed comparisons than those obtained here are not possible in the absence of detailed data in the vicinity of the wavemaker ($x < 8$ m).

Finally, the evolution process described in the present cases occurs in the space of about two first harmonic wavelengths, indicating that the theoretical limitation to slowly varying topography and amplitudes is not restrictive in practice.

Concluding Remarks

The present study has demonstrated that the parabolic equation method may be successfully applied to the modeling of weakly nonlinear, weakly dispersive wave motions governed by the Boussinesq equations. The present study has been confined to the investigation of the propagation of monochromatic waves together with their nonlinearly-generated harmonics. However, given the necessary computer capacity, the method is directly applicable to the problem of modeling two-dimensional spectral evolution in shallow water.

In this study we have neglected the effects of frictional dissipation and wave breaking; the models in their present form are thus applicable to the region seaward of the surf zone. The inclusion of wave breaking effects in the models may be expected to be a non-trivial extension of the present results, since the models do not directly calculate the total wave height at each computational point.

Acknowledgements

This research was carried out with the support of the Office of Naval Research, Coastal Sciences Program (JTK and RAD) and New York Sea Grant Institute (PLFL and SBY). The possible utility of the K-P equation in the study of combined refraction and diffraction was suggested by Dr. J. L. Hammack.

This is contribution No. 434 of the Marine Science Research Center.

Appendix 1 References

1. Booij, N., 1981, "Gravity waves on water with non-uniform depth and current," Rept. 81-1, Dept. Civil Engrg., Delft University of Technology.
2. Bryant, P. J., 1982, "Two-dimensional periodic permanent waves in shallow water," J. Fluid Mech. 115, 525-532.
3. Dalrymple, R. A., Kirby, J. T., & Hwang, P. A., 1984, "Wave diffraction due to areas of energy dissipation," J. Waterway, Port, Coastal and Ocean Engineering, ASCE, 110, 67-79.
4. Johnson, R. S., 1972, "Some numerical solutions of a variable-coefficient Korteweg-deVries equation (with applications to solitary wave development on a shelf)," J. Fluid Mech. 54, 81-91.
5. Kadomtsev, B. B. and Petviashvili, V. I., 1970, "On the stability of solitary waves in weakly dispersing media," Sov. Phys. Dokl. 15, 539-541.
6. Kirby, J. T., 1984, "A note on linear surface wave-current interaction over slowly varying topography," J. Geophys Res. 89, 745-747.
7. Kirby, J. T., 1984, "On the gradual reflection of weakly-nonlinear Stokes waves in regions with slowly varying topography," submitted for publication.
8. Kirby, J. T. and Dalrymple, R. A., 1983, "A parabolic equation for the combined refraction-diffraction of Stokes waves by mildly varying topography," J. Fluid Mech., 136, 453-466.
9. Liu, P. L-F., 1983, "Wave-current interactions on a slowly varying topography," J. Geophys. Res. 88, 4421-4426.
10. Liu, P. L-F. and Tsay, T.-K., 1983, "On weak reflection of water waves," J. Fluid Mech. 131, 59-71.
11. Liu, P. L-F. and Tsay, T.-K., 1984, "Refraction-diffraction model for weakly nonlinear water waves," J. Fluid Mech. 141, 265-274.
12. Lozano, C. and Liu, P. L-F., 1980, "Refraction-diffraction model for linear surface water waves," J. Fluid Mech. 101, 705-720.
13. Madsen, P. A. and Warren, I. R., 1984, "Performance of a numerical short-wave model," Coastal Engineering 8, 73-79.
14. Radder, A. C., 1979, "On the parabolic equation method for water-wave propagation," J. Fluid Mech. 95, 159-176.
15. Rogers, S. R. and Mei, C. C., 1978, "Nonlinear resonant excitation of a long and narrow bay," J. Fluid Mech. 88, 161-180.
16. Skovgaard, O., Jonsson, I. G. & Bertelsen, J. A., 1975, "Computation of wave heights due to refraction and friction," J. Waterways, Port, Harbors and Coastal Engineering Div., ASCE, 101, 15-32.
17. Skovgaard, O. and Petersen, H. M., 1977, "Refraction of cnoidal waves," Coastal Engrg. 1, 43-61.
18. Whalin, R. W., 1971, "The limit of applicability of linear wave refraction theory in a convergence zone," Res. Rep. H-71-3, U.S. Army Corps of Engrs., Waterways Expt. Station, Vicksburg, MS.
19. Yue, D. K. P. and Mei, C. C., 1980, "Forward diffraction of Stokes waves by a thin wedge," J. Fluid Mech. 99, 33-52.